

Bright photoactivatable fluorophores for single-molecule imaging

Jonathan B Grimm^{1,2}, Brian P English^{1,2}, Heejun Choi¹, Anand K Muthusamy¹, Brian P Mehl¹, Peng Dong¹, Timothy A Brown¹, Jennifer Lippincott-Schwartz¹, Zhe Liu¹, Timothée Lionnet¹ & Luke D Lavis¹

Small-molecule fluorophores are important tools for advanced imaging experiments. We previously reported a general method to improve small, cell-permeable fluorophores which resulted in the azetidine-containing ‘Janelia Fluor’ (JF) dyes. Here, we refine and extend the utility of these dyes by synthesizing photoactivatable derivatives that are compatible with live-cell labeling strategies. Once activated, these derived compounds retain the superior brightness and photostability of the JF dyes, enabling improved single-particle tracking and facile localization microscopy experiments.

Small-molecule fluorophores are brighter than fluorescent proteins and remain a crucial element of modern microscopy methods^{1,2}. The development of new protein-specific labeling strategies, such as the self-labeling tag concept pioneered by Johnsson^{3,4}, enables the formation of fluorescent bioconjugates inside living cells; membrane-permeable synthetic dye ‘ligands’ passively diffuse into cells where they form covalent bonds with their cognate protein ‘tags’. Self-labeling tag systems thus combine genetic encoding—one of the main advantages of fluorescent proteins—with the favorable photophysics of organic fluorophores. Building upon these sophisticated attachment techniques, we recently reported that incorporation of four-membered azetidine rings could substantially improve the brightness and photostability of small, cell-permeable fluorophores⁵. These JF dyes are excellent labels for live-cell imaging, especially in single-molecule tracking experiments where they enable longer observations and better localization of individual fluorescent conjugates. We now report photoactivatable (PA) versions of JF₅₄₉ and JF₆₄₆, demonstrate their compatibility with existing live-cell labeling strategies, and show their utility in single-molecule tracking and super-resolution imaging.

Our laboratory has developed efficient synthetic strategies to prepare photoactivatable rhodamines by N-acylation with standard photolabile ‘cages’^{6,7}. Most caging groups are large and hydrophobic, however, and these characteristics diminish their

solubility and reactivity with self-labeling tag proteins. Moreover, classic photocaging strategies are incompatible with fully N-alkylated rhodamine dyes such as JF₅₄₉ and JF₆₄₆. To circumvent these issues, we used a caging strategy serendipitously discovered by Hell and coworkers, in which treatment of rhodamine dyes with oxalyl chloride and diazomethane generates a spirocyclic diazoketone that is colorless and nonfluorescent⁸. Activation of these molecules with short-wavelength light elicits a large increase in fluorescence. Although diazoketone-caged dyes have been employed as antibody labels for fixed-cell imaging, this type of photoactivatable dye has neither been incorporated into self-labeling tag systems nor used in live cells.

To test the compatibility of this caging strategy with the azetidinyl JF dyes, we first prepared the photoactivatable JF₅₄₉ (PA-JF₅₄₉, **2**) in good yield from JF₅₄₉ (**1**; Fig. 1a)⁵. We then evaluated the photochemistry of PA-JF₅₄₉ (**2**) in water; previous reports had only described the photolysis of diazoketone-caged dyes in methanol⁸. Surprisingly, the major product from exhaustive photolysis of compound **1** in aqueous solution was not the expected phenylacetic acid dye **3** but rather the methyl-substituted JF₅₄₉ (**4**) along with the putative nonfluorescent ‘dark product’ **5** (Fig. 1a). Compound **4** was generated with an apparent photochemical quantum yield (Φ_{PC}) value of 2.2% (Supplementary Note), similar to that of photoswitchable fluorescent proteins ($\Phi_{PC} \approx 1\%$)⁹. This unexpected compound **4** was produced by efficient ($\Phi_{PC} = 15\%$) photoinduced decarboxylation¹⁰ of the initial photochemical product **3** (Supplementary Note). Nevertheless, the two photo-products **3** and **4** were highly fluorescent molecules with similar spectral properties to those of the parent JF₅₄₉ (**1**; Fig. 1b). As reported⁵, fluorophore **1** exhibited an absorption maximum (λ_{max}) of 549 nm, extinction coefficient (ϵ) of $1.01 \times 10^5 \text{ M}^{-1}\text{cm}^{-1}$, emission maximum (λ_{em}) of 571 nm, and a fluorescence quantum yield (Φ_F) of 0.88. Fluorophore **3** showed $\lambda_{max}/\lambda_{em} = 553 \text{ nm}/573 \text{ nm}$, and it retained 95% of the brightness of **1** ($\epsilon = 9.89 \times 10^4 \text{ M}^{-1}\text{cm}^{-1}$; $\Phi_F = 0.85$); whereas dye **4** gave $\lambda_{max}/\lambda_{em} = 551 \text{ nm}/570 \text{ nm}$, and it retained 75% of the brightness of **1** ($\epsilon = 8.59 \times 10^4 \text{ M}^{-1}\text{cm}^{-1}$; $\Phi_F = 0.78$).

Encouraged by the brightness of the PA-JF₅₄₉ photoproducts, we synthesized the HaloTag ligand¹¹ of PA-JF₅₄₉ (**6**; Fig. 1c and Supplementary Note). Labeling of HaloTag protein with **6** either *in vitro*, in live cells, or in fixed cells produced conjugates with low background absorption and fluorescence that could be activated by one- or two-photon illumination (Supplementary Fig. 1a and Supplementary Videos 1–3). We found that attachment of **6** to the HaloTag improves the yield of the desired fluorescent products compared to the yield from the free PA-JF₅₄₉ ligand (Supplementary Fig. 1b,c), perhaps by restricting conformational flexibility and preventing the formation of the planar dark

¹Janelia Research Campus, Howard Hughes Medical Institute, Ashburn, Virginia, USA. ²These authors contributed equally to this work. Correspondence should be addressed to T.L. (lionnett@janelia.hhmi.org) or L.D.L. (lavisl@janelia.hhmi.org).

RECEIVED 4 APRIL; ACCEPTED 20 SEPTEMBER; PUBLISHED ONLINE 24 OCTOBER 2016; DOI:10.1038/NMETH.4034

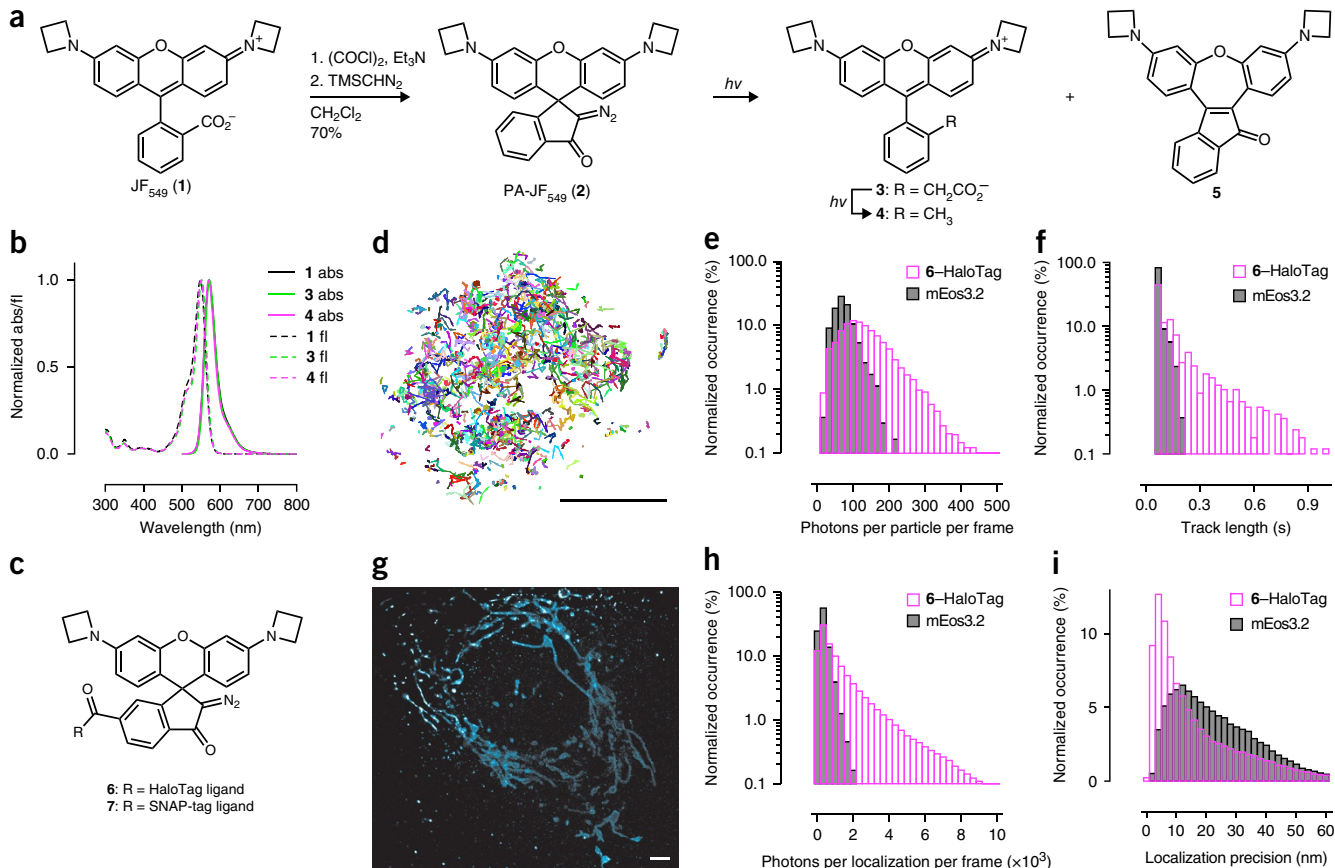


Figure 1 | Synthesis, characterization, and utility of photoactivatable Janelia Fluor 549 (PA-JF₅₄₉). **(a)** Synthesis and photochemistry of PA-JF₅₄₉. Treatment of JF₅₄₉ (**1**) with oxalyl chloride (COCl)₂ and triethylamine (Et₃N), followed by TMS diazomethane (TMSCHN₂) in dichloromethane yields PA-JF₅₄₉ (**2**) in 70% yield. Photoactivation (*hν*, 365 nm) yields only a trace amount of the expected phenylacetic acid derivative (CH₂CO₂⁻) (**3**) with methyl (CH₃)-substituted JF₅₄₉ (**4**) as the major product (50%) and the indanone **5** as the minor (10%) product. **(b)** Normalized absorption (abs) and fluorescence emission (fl) spectra of **1**, **3**, and **4**. **(c)** Chemical structure of PA-JF₅₄₉-HaloTag ligand (**6**) and PA-JF₅₄₉-SNAP-tag ligand (**7**). **(d)** Image of cumulative single-particle tracks of HaloTag–Sox2 labeled with PA-JF₅₄₉ ligand **6**; scale bar, 5 μm. **(e)** Histogram of detected photons per particle per frame when performing sptPALM of Sox2 using the **6**–HaloTag fusion (magenta, median = 120.7 photons) or mEos3.2 fusion (black, median = 70.9 photons) under identical imaging conditions. **(f)** Histogram of track length when performing sptPALM of Sox2 using the **6**–HaloTag fusion (magenta, mean = 0.20 s) or mEos3.2 fusion (black, mean = 0.07 s) under identical imaging conditions. **(g)** PALM image of U2OS cell expressing TOMM20–HaloTag and labeled with PA-JF₅₄₉ ligand **6**; the 268,561 detected molecules are displayed according to their localization full width at half maximum; scale bar, 2 μm. **(h)** Histogram of detected photons per localization per frame when performing PALM of TOMM20 using the **6**–HaloTag fusion (magenta, median = 636.6 photons) or mEos3.2 fusion (black, median = 266.8 photons) under identical imaging conditions. **(i)** Histogram of calculated localization precision when performing PALM of TOMM20 using the **6**–HaloTag fusion (magenta, median = 13.5 nm) or mEos3.2 fusion (black, median = 20.2 nm) under identical imaging conditions.

product **5** (Fig. 1a). This enhancement in desired photochemical outcome upon conjugation to protein was also observed for the PA-JF₅₄₉-SNAP-tag ligand (**7**; Fig. 1c and Supplementary Fig. 1d–f). Although advantageous, this improvement in photochemistry upon conjugation was not large enough to eliminate the need for washing out free ligand.

We directly compared the performance of the PA-JF₅₄₉-HaloTag ligand (**6**) to the genetically encoded fluorescent protein mEos3.2 (ref. 12). The activation rate of PA-JF₅₄₉ (τ = 94.5 s) was similar to that of mEos3.2 (τ = 107 s; Supplementary Fig. 1g). The on/off activation ratios¹³ were also similar (~10⁻⁵; Supplementary Fig. 1h and Supplementary Table 1) between the two. The median number of detected photons per localization was higher for PA-JF₅₄₉ than mEos3.2 (JF₅₄₉ = 870.9, mEos3.2 = 533.7; Supplementary Fig. 1i). We then compared the dyes in single-particle tracking photoactivated localization microscopy (sptPALM)¹⁴ experiments in live mouse embryonic stem (ES) cells expressing HaloTag–Sox2 or

mEos3.2–Sox2 fusions (Fig. 1d and Supplementary Video 4). The PA-JF₅₄₉ showed a sizeable improvement in performance compared with the mEos3.2 fluorophore, giving higher detected photons per particle per frame (median = 120.7) and longer tracks (mean = 0.20 s) than mEos3.2 (median detected photons per particle per frame = 70.9; mean track length = 0.07 s; Fig. 1e,f). We also compared ligand **6** to the commercially available tetramethylrhodamine (TMR) HaloTag ligand¹¹ (**9**; Supplementary Fig. 1b,j) using a multifocus microscope (MFM)¹⁵ setup where we observed superior performance of the PA-JF₅₄₉ ligand in 3D tracking (Supplementary Fig. 1j–o and Supplementary Video 5).

We then tested the utility of PA-JF₅₄₉-HaloTag ligand as a label for PALM¹⁶ in fixed cells. We imaged mitochondrial protein TOMM20 fused to either mEos3.2 (Supplementary Fig. 1p) or the HaloTag protein and labeled the HaloTag fusions with ligand **6** (Fig. 1g). As expected (Supplementary Fig. 1i), the PA-JF₅₄₉-HaloTag conjugate gave higher photon counts per localization

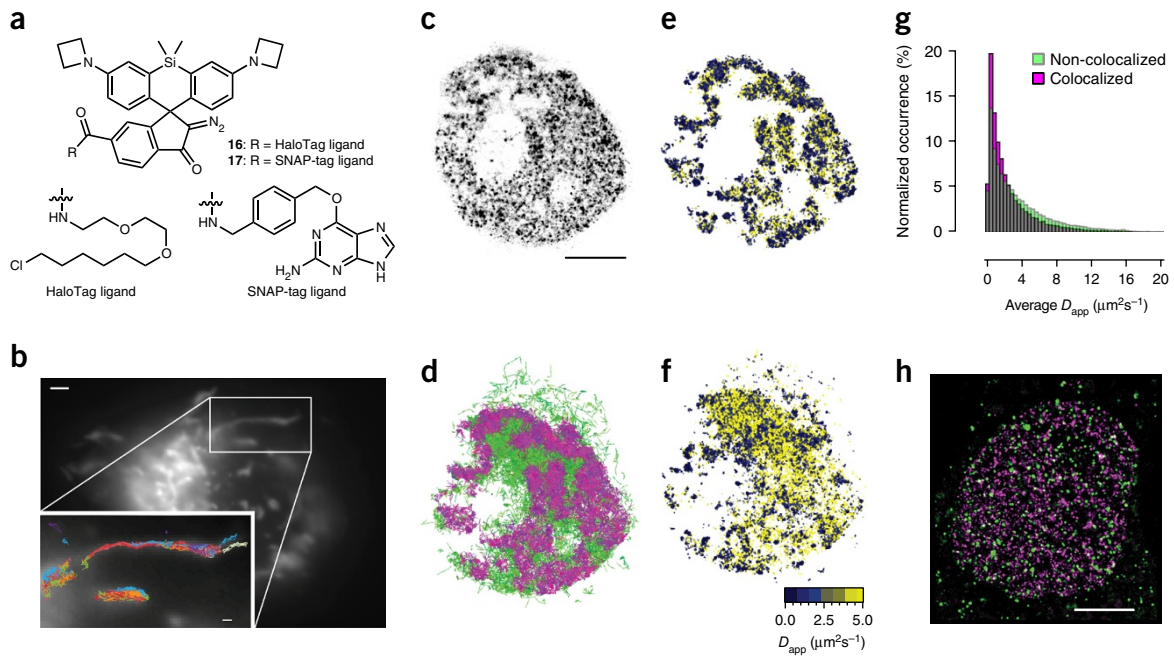


Figure 2 | Multicolor imaging using photoactivatable Janelia Fluor 646 (PA-JF₆₄₆). **(a)** Structures of PA-JF₆₄₆-HaloTag ligand (**16**) and PA-JF₆₄₆-SNAP-tag ligand (**17**). **(b)** Image of U2OS cell expressing TOMM20-HaloTag and labeled with 10 nM JF₅₄₉-HaloTag ligand **8** and 10 nM PA-JF₆₄₆-HaloTag ligand **16**. The spatial distribution of the widefield fluorescence microscopy image from JF₅₄₉-HaloTag ligand **8** resembles typical mitochondrial distribution in a cell (scale bar, 5 μ m). The tracks ($n = 154$, various colors) of single TOMM20 fusions labeled with PA-JF₆₄₆ are plotted on the averaged widefield TOMM20-JF₅₄₉ signal (inset; scale bar, 1 μ m). The majority of single-molecule trajectories (>95%) colocalize with the JF₅₄₉-HaloTag signal, indicating specific labeling of PA-JF₆₄₆. **(c–g)** Simultaneous two-color sptPALM experiment in a live ES cell expressing histone H2B-SNAP-tag labeled with **17** and HaloTag-Sox2 labeled with PA-JF₅₄₉-HaloTag ligand **6**. **(c)** PALM image of histone H2B-SNAP-tag labeled with **17**; scale bar, 5 μ m. **(d)** Single-particle trajectories of HaloTag-Sox2 that are colocalized with histone H2B-SNAP-tag (6,272 trajectories; magenta) or noncolocalized with histone H2B-SNAP-tag (7,081 trajectories; green). **(e)** Apparent diffusion coefficient (D_{app}) map of colocalized fraction of Sox2. **(f)** Apparent diffusion coefficient map of noncolocalized fraction of Sox2. **(g)** Histogram of apparent diffusion coefficient calculated for each step in the colocalized and noncolocalized Sox2 trajectories. **(h)** Overlay of the PALM image of Htt84Q-mEos3.2-nuclear localization signal (NLS) clusters with the PALM image of histone H2B-HaloTag labeled with **16**. The PALM images were simultaneously recorded and are each composed of 10,000 consecutive frames. The 128,740 detected mEos3.2 molecules (green) and the 739,964 PA-JF₆₄₆ molecules (magenta) are displayed according to their localization full width at half maximum; the areas of overlap between these two molecules result in white spots. The median number of detected photons per mEos3.2 molecule per frame was 115.6, and the median number of detected photons per PA-JF₆₄₆ molecule per frame was 757.6. The median calculated localization error for mEos3.2 was 34.5 nm, and for PA-JF₆₄₆ it was 21.3 nm. Scale bar, 5 μ m.

event per frame (median = 636.6) and calculated localization precision (median $\sigma = 13.5$ nm) compared with mEos3.2 (median detected photons per localization per frame = 266.8; median $\sigma = 20.2$ nm; **Fig. 1h,i**). We also confirmed the dyes could function as PALM labels with other HaloTag fusions in different cellular regions (**Supplementary Fig. 1q-s** and **Supplementary Video 6**). Overall, the PA-JF₅₄₉ label gave relatively high photon counts, and calculated localization precision and showed only modest blinking (**Supplementary Fig. 1t-v**). Nevertheless, the use of genetically encoded self-labeling tags does not address issues with labeling density—a key determinant of image quality in localization microscopy¹⁷.

We then set out to perform two-color sptPALM, an experiment that has been stymied by the scarcity of two spectrally distinct photoactivatable fluorophores. We reasoned that the use of the same diazoketone caging strategy on different JF dyes could allow sparse photoactivation of both labels with similar efficiency, thus facilitating two-color experiments. We first converted JF₆₄₆ (**11**) into the photoactivatable JF₆₄₆ (PA-JF₆₄₆, **12**; **Supplementary Fig. 2a** and **Supplementary Note**) to test whether this caging strategy would be compatible with the Si-rhodamine scaffold. Interestingly, photolysis of the free PA-JF₆₄₆ **12** gave only small amounts

(<5%) of the expected fluorophores **13** and **14**, with the major product being the nonfluorescent **15** (**Supplementary Fig. 2a** and **Supplementary Note**). Nevertheless, based on the ‘on-protein’ improvement in photochemistry observed for the PA-JF₅₄₉ compounds (**Supplementary Fig. 1a-f**), we predicted that PA-JF₆₄₆ would show better performance as a photoactivatable fluorophore when conjugated. Accordingly, we synthesized the HaloTag and SNAP-tag ligands of PA-JF₆₄₆ (**16** and **17**, respectively; **Fig. 2a** and **Supplementary Note**). These compounds showed substantial improvements in photochemical outcome upon binding to their cognate proteins (**Supplementary Fig. 2b-e** and **Supplementary Note**) and a high activation rate ($\tau = 83.5$; **Supplementary Fig. 2f**) in live cells. The on/off ratio was substantially lower ($\sim 10^{-6}$) on account of the lower rate of spontaneous activation under the red excitation light (**Supplementary Fig. 2g** and **Supplementary Table 1**). The low background staining exhibited with PA-JF₅₄₉ ligand **6** was also observed with the PA-JF₆₄₆-HaloTag ligand **16** (**Supplementary Fig. 2h,i**), allowing sptPALM in live cells (**Fig. 2b** and **Supplementary Video 7**).

To further validate the PA-JF₅₄₉ and PA-JF₆₄₆ pair for two-color sptPALM, we expressed the transcription factor Sox2 as a fusion with HaloTag protein and labeled this fusion with PA-JF₅₄₉-HaloTag

ligand **6**. We coexpressed histone H2B as a fusion with the SNAP-tag and labeled this population with PA-JF₆₄₆-SNAP-tag ligand (17); these photoactivatable dyes allowed simultaneous tracking of both H2B and Sox2 by photoactivation with 405-nm light. We generated a map of histone H2B locations using a standard PALM analysis (**Fig. 2c**) and defined Sox2 trajectories that were either colocalized or not colocalized with the areas of high density in the chromatin PALM map (**Fig. 2d**). As expected, the molecules of Sox2 that were colocalized with histone H2B exhibited slower diffusion coefficients than did the noncolocalized fraction (**Fig. 2e–g** and **Supplementary Fig. 2j,k**).

Finally, we investigated the PA-JF₆₄₆ label for multicolor localization microscopy. Although a few self-labeling tag ligands have been used for PALM imaging^{8,18,19}, previously reported molecules exhibit relatively short emission maxima and are thus incompatible with other localization microscopy labels such as photoconvertible fluorescent proteins. Based on our previous work with another caged Si-rhodamine with similar wavelengths⁷, we reasoned that PA-JF₆₄₆ would be red shifted enough to be useful for two-color PALM with mEos3.2. We first showed that PA-JF₆₄₆-HaloTag ligand **16** could be used for one-color PALM in cells expressing HaloTag–vimentin or HaloTag–TOMM20 fusions (**Supplementary Fig. 2l,m**). The calculated localization precision in the TOMM20 image using PA-JF₆₄₆ ligand **16** was similar to that of PA-JF₅₄₉ (median $\sigma = 13.8$ nm; **Fig. 1i** and **Supplementary Fig. 2n**). For a two-color experiment, we expressed histone H2B as a fusion with the HaloTag, labeling with PA-JF₆₄₆-HaloTag ligand **16** and the mutant Huntington protein Htt-94Q as a fusion with mEos3.2. After labeling, fixation, and two-color PALM (**Fig. 2h**), we observed that histone H2B (magenta) and Htt-94Q aggregates (green) only rarely overlapped (i.e., few white spots), which supports the hypothesis that the aggregates formed by expanded polyglutamine domains displace chromatin structures in the nucleus²⁰.

In conclusion, we report photoactivatable versions of the bright, photostable JF dyes. These fluorophores retain the superior photon yields, membrane permeability, and utility in live cells exhibited by the fluorescent JF dyes but have the added benefit of photoactivation, allowing sophisticated sptPALM experiments. These dyes also constitute a useful addition to the expanding palette of PALM labels for fixed cells. In particular, PA-JF₆₄₆ is the first far-red photoactivatable fluorophore compatible with live-cell labeling using the HaloTag or SNAP-tag systems, allowing multicolor single-particle tracking experiments and super-resolution microscopy. We expect these small and bright photoactivatable labels to be compatible with many different labeling strategies, therefore extending the boundaries of single-molecule imaging in live and fixed

cells. Beyond localization microscopy, these versatile labels should provide a favorable alternative to photoconvertible fluorescent proteins in any imaging experiment where photoactivation is used to highlight a specific cell or cellular region.

METHODS

Methods and any associated references are available in the [online version of the paper](#).

Note: Any Supplementary Information and Source Data files are available in the [online version of the paper](#).

ACKNOWLEDGMENTS

We thank W. Legant and E. Betzig for contributive discussions; H. White, D. Walpita, K. Schaefer, and P. Nguyen for assistance with molecular biology and cell culture; and A. Berro, A. Abdelfattah, and E. Schreiter (all at Janelia) for the purified HaloTag and SNAP-tag proteins. This work was supported by the Howard Hughes Medical Institute.

AUTHOR CONTRIBUTIONS

J.B.G., B.P.E., Z.L., T.L., and L.D.L. conceived the project. J.B.G. contributed organic synthesis and photochemistry experiments; B.P.E., H.C., B.P.M., P.D., and T.A.B. contributed cell biological experiments and data analysis; A.K.M. contributed organic synthesis; J.L.-S., Z.L., T.L., and L.D.L. directed the project and contributed data analysis. L.D.L. wrote the paper with input from the other authors.

COMPETING FINANCIAL INTERESTS

The authors declare competing financial interests: details are available in the [online version of the paper](#).

Reprints and permissions information is available online at <http://www.nature.com/reprints/index.html>.

1. Lavis, L.D. & Raines, R.T. *ACS Chem. Biol.* **3**, 142–155 (2008).
2. Lavis, L.D. & Raines, R.T. *ACS Chem. Biol.* **9**, 855–866 (2014).
3. Keppler, A. *et al.* *Nat. Biotechnol.* **21**, 86–89 (2003).
4. Xue, L., Karpenko, I.A., Hiblot, J. & Johnsson, K. *Nat. Chem. Biol.* **11**, 917–923 (2015).
5. Grimm, J.B. *et al.* *Nat. Methods* **12**, 244–250 (2015).
6. Grimm, J.B. *et al.* *ACS Chem. Biol.* **8**, 1303–1310 (2013).
7. Grimm, J.B. *et al.* *Angew. Chem. Int. Ed. Engl.* **55**, 1723–1727 (2016).
8. Belov, V.N. *et al.* *Chemistry* **20**, 13162–13173 (2014).
9. Habuchi, S., Tsutsui, H., Kochaniak, A.B., Miyawaki, A. & van Oijen, A.M. *PLoS One* **3**, e3944 (2008).
10. Epling, G.A. & Lopes, A. *J. Am. Chem. Soc.* **99**, 2700–2704 (1977).
11. Los, G.V. *et al.* *ACS Chem. Biol.* **3**, 373–382 (2008).
12. Zhang, M. *et al.* *Nat. Methods* **9**, 727–729 (2012).
13. Wang, S., Moffitt, J.R., Dempsey, G.T., Xie, X.S. & Zhuang, X. *Proc. Natl. Acad. Sci. USA* **111**, 8452–8457 (2014).
14. Manley, S. *et al.* *Nat. Methods* **5**, 155–157 (2008).
15. Abrahamsson, S. *et al.* *Nat. Methods* **10**, 60–63 (2013).
16. Betzig, E. *et al.* *Science* **313**, 1642–1645 (2006).
17. Legant, W.R. *et al.* *Nat. Methods* **13**, 359–365 (2016).
18. Lee, H.D. *et al.* *J. Am. Chem. Soc.* **132**, 15099–15101 (2010).
19. Banala, S., Maurel, D., Manley, S. & Johnsson, K. *ACS Chem. Biol.* **7**, 289–293 (2012).
20. Li, L. *et al.* *eLife* **5**, e17056 (2016).

ONLINE METHODS

Chemical synthesis and photochemistry. Experimental details and characterization for all novel compounds and subsequent spectroscopy and photochemistry experiments can be found in the **Supplementary Note**.

UV-vis and fluorescence spectroscopy. Spectroscopy was performed using 1-cm-path-length quartz cuvettes. All measurements were taken at ambient temperature ($22 \pm 2^\circ\text{C}$). Absorption spectra were recorded on a Cary Model 100 spectrometer (Agilent). Fluorescence spectra were recorded on a Cary Eclipse fluorometer (Varian). Absolute fluorescence quantum yields (Φ_F) for all fluorophores were measured using a Quantaurus-QY spectrometer (model C11374, Hamamatsu).

General microscopy methods. A comprehensive listing of instrument parameters for all imaging experiments can be found in **Supplementary Table 2**. Additional information is given below.

Cell culture. Mouse D3n embryonic stem (ES) cells (ATCC) were maintained on 0.1% w/v gelatin-coated plates in the absence of feeder cells. The ES cell medium was prepared by supplementing knockout Dulbecco's modified eagles media (DMEM, Invitrogen) with 15% v/v fetal bovine serum (FBS), 1 mM GlutaMAX, 0.1 mM nonessential amino acids, 1 mM sodium pyruvate, 0.1 mM 2-mercaptoethanol, and 1,000 units of leukemia inhibitory factor (LIF; Millipore). U2OS (ATCC) and COS-7 (ATCC) cells were cultured in DMEM (Corning) with 10% v/v FBS supplemented with 2 mM L-glutamine or 2 mM GlutaMAX. Cells were regularly tested for mycoplasma contamination by the Janelia Cell Culture Facility.

Plasmid construction. Sox2 and histone H2B cDNA were amplified from ES cell cDNA libraries. Htt-94Q cDNA was obtained from Addgene (plasmid #23966). The full-length cDNAs were cloned into the Piggybac transposon vector (PB533A-2, System Biosciences) or a modified Piggybac transposon vector with PuroR. The sequence for HaloTag (Promega) or mEos3.2 (Addgene, plasmid #54525) was ligated inframe with the cDNA of the desired proteins at the N terminus (HaloTag–Sox2) or C terminus (histone H2B–HaloTag, histone H2B–SNAP-tag, and Htt-94Q–mEos3.2-NLS). The plasmids coding ensconsin–HaloTag, clathrin–HaloTag, TOMM20–HaloTag, Sec61 β –HaloTag, and vimentin–HaloTag were constructed by substituting the sequence for the HaloTag for the sequence of mEmerald in a collection of plasmids that were a generous gift from M. Davidson (Florida State). Each plasmid was transiently transfected into U2OS cells using the Nucleofector Kit (Lonza).

Stable cell line generation. Stable cell lines were generated by cotransfection of Piggybac transposon vector with a helper plasmid that overexpresses Piggybac transposase (Super Piggybac Transposase, System Biosciences). At 48 h post-transfection, cells were subjected to neomycin or puromycin (Invitrogen) selection. Transfection was conducted by using the Nucleofector system (Lonza).

ES cell labeling strategy and preparation for imaging. 1 d before imaging, ES cells were plated onto a cover slip precoated

with iMatrix-511 (Clontech). Imaging was performed in the ES cell imaging medium, which was prepared by supplementing FluoroBrite medium (Invitrogen) with 10% v/v FBS, 1 mM glutamax, 0.1 mM nonessential amino acids, 1 mM sodium pyruvate, 10 mM HEPES (pH 7.2–7.5), 0.1 mM 2-mercaptoethanol, and 1,000 units of LIF (Millipore). For PA-JF₅₄₉ or PA-JF₆₄₆ labeling, cells were incubated with PA-JF₅₄₉-HaloTag ligand (6) or PA-JF₆₄₆-HaloTag ligand (16) at a final concentration of 100 nM for 1 h. For the two-color sptPALM live-cell tracking experiments, labeled cells were washed with ES cell imaging medium (3×) before imaging. For the two-color fixed-cell PALM imaging experiments, labeled cells were washed with PBS (4×), fixed in 4% w/v paraformaldehyde for 10 min, and washed with PBS (3×). The final PALM imaging was performed in PBS solution.

3D spt-dSTORM and spt-PALM tracking experiments. Fluorescently tagged HaloTag–Sox2 molecules labeled either with PA-JF₅₄₉-HaloTag ligand (6) or with TMR-HaloTag ligand (9) were tracked in live ES cells in 3D using a custom-built multifocus microscope¹⁵. The fluorescence from nine focal planes was simultaneously recorded using an iXon Ultra EMCCD camera (DU-897U-CS0-#BV, 17 MHz EM amplifiers, preamp setting 1, Gain 300) at a frame time of 30 ms.

One-color PALM labeling and fixation. Cells were grown on precleaned 25-mm-diameter coverslips or precleaned 25-mm-diameter coverslips embedded with gold-nanorods as fiducial markers (generous gift from G. Shtengel, Janelia). Before fixation, cells were labeled with 10 nM of the HaloTag ligand for 30 min at 37 °C, 5% CO₂. Cells were then washed three times with prewarmed DMEM buffer containing 10% FBS. Before fixation, the coverslips were washed twice with prewarmed PBS solution without magnesium chloride or calcium chloride. 1 mL of 8% formaldehyde solution in PBS was slowly added to a dish containing 1 mL of PBS, and the resulting 4% formaldehyde solution was incubated at room temperature for 10 min. The coverslips were washed twice with PBS and incubated in 0.1% v/v Triton X-100 in PBS solution for 4 min. The coverslips were washed twice in PBS and then incubated in 1% w/v BSA in PBS for 1 h at ambient temperature. After washing twice more with PBS, the coverslips were mounted into metal cell chambers for PALM imaging.

Two color sptPALM live-cell tracking experiments. ES cells expressing both HaloTag–Sox2 fusions labeled with PA-JF₅₄₉-HaloTag ligand (6) and SNAP-tag–histone H2B fusions labeled with PA-JF₆₄₆-SNAP-tag ligand (17) were tracked simultaneously using a custom-built three-camera microscope²¹. Two iXon Ultra EMCCD cameras (DU-897-CS0-BV and DU-897U-CS0-EXF, both cooled to –80 °C, 17 MHz EM amplifiers, preamp setting 3, Gain 400) were synchronized using a National Instruments DAQ board (NI-DAQ-USB-6363) at a frame time of 10 ms. 5 ms stroboscopic excitations of a 555 nm laser (CL555-1000-O with TTL modulation, CrystaLaser) and a 639 nm laser (Stradus 637-140, Vortran) were synchronized to the frame times of the two respective cameras via LabVIEW 2012 (National Instruments). The two lasers stroboscopically illuminated the sample using peak power densities of ~1.7 kW/cm² using HiLo illumination of the nucleus. The PA-JF₅₄₉ and PA-JF₆₄₆ labels were photoconverted by 100-μs-long excitation pulses of 407 nm light (50 W/cm²) every

second. During the course of image acquisition, the pulse length was increased to 200- μ s-long pulses. During imaging, cells were maintained at 37 °C and 5% CO₂ using a Tokai-hit stage top incubator and objective heater²¹. We determined colocalized Sox2 and histone H2B trajectories in our live-cell experiment using a previously published analysis^{5,22}. Briefly, we localized particles and built trajectories in both channels separately. Trajectories that dwelled within 320 nm of one another for at least 10 ms were assigned as colocalized. We then calculated diffusion coefficient maps and histograms as described in Grimm *et al.*⁵.

Determination of background staining. COS-7 cells were stably transfected with a plasmid expressing a human histone H2B-HaloTag protein fusion. Untransfected COS-7 cells and the stable histone H2B-HaloTag-expressing cells were plated into 35 mm MatTek glass-bottom dishes at 2 × 10⁵ cells per plate in phenol-red-free DMEM with 10% FBS and GlutaMAX. After 24 h, cells were rinsed with PBS and fixed with 2 mL of fresh 4% w/v paraformaldehyde in 0.1 M phosphate buffer, pH 7.4 for 30 min, followed by two washes with PBS. The histone H2B-HaloTag protein was stained with 100 nM of either PA-JF₅₄₉-HaloTag ligand (**6**) or PA-JF₆₄₆-HaloTag ligand (**16**) for 30 min along with 5 μ g/mL Hoechst 33342 (Invitrogen) in PBS. The cells were then washed twice with PBS, washed for 20 min with PBS containing 0.1% v/v Triton X-100 and 3% w/v BSA, followed by two more washes with PBS. Cells were imaged using a Zeiss 710 LSM. Z-dimension stack boundaries were set using the Hoechst 33342 nuclear-reference stain, which was imaged using 405 nm excitation and 410–485 nm emission. Partial photoactivation of PA-JF₅₄₉ and PA-JF₆₄₆ was accomplished with 60 iterations of 405 nm set at 75% laser power. Images for activated JF₅₄₉ were collected using 561 nm excitation and 566–685 nm emission. Images for JF₆₄₆ were collected using 633 nm excitation and 638–759 nm emission. The Hoechst 33342 and JF dye tracks were collected separately. Image analysis was done using Fiji. Confocal stacks are displayed as maximum projection images. The experimental and control images were set to the same brightness/contrast scales.

Two-color fixed-cell PALM imaging acquisition. ES cells expressing both Htt94Q-mEos3.2 and histone H2B-HaloTag labeled with PA-JF₆₄₆-HaloTag ligand (**16**) were imaged using the previously described custom-built 3-camera microscope at a frame time of 50 ms and a constant illumination power density of around 4 kW/cm² for both 555 nm and 639 nm excitation lasers. mEos3.2 and PA-JF₆₄₆ were photoconverted by 100 μ s long excitation pulses of 407 nm light (100 W/cm²) every second. The mEos3.2 emitted 115.6 detected photons/localization/frame and molecules emit on average for 4 frames, as determined by tracking using stringent displacement parameters to select immobile particles. Thus, each mEos3.2 emits approximately 460 detected photons, consistent with literature reports¹³. The 1.7-fold higher resolution enhancement afforded by JF₆₄₆ is smaller than expected based on the 6.5-fold more detected photons/localization/frame (757.6) and the red-shifted spectra of JF₆₄₆. This is primarily due to the camera pixel size being optimized for the dimmer protein fluorophore and the increased fluorescence background generated by bright out-of-focus JF₆₄₆ molecules.

PALM and sptPALM tracking image analysis. For simultaneous two-camera imaging and tracking, the two 16-bit TIFF stacks were

registered using the similarity (2d) transformation model using a descriptor-based Fiji plugin²³. Super-resolution images were rendered using the software package Localizer by Dedecker *et al.*²⁴ with eight-way adjacency particle detection, 20 GLRT sensitivity, and a PSF of 1.3 pixels. The following settings were chosen for particle track linking: five-pixel maximum jump distance, three-frame minimum track length, and 15 GLRT sensitivity. Resulting tracks were then exported as text files, and diffusion mapping was performed with code written in Igor Pro 6.36 (WaveMetrics). The code calculates local apparent diffusion coefficients evaluated in 20 nm by 20 nm grids from the mean square displacements over the frame-time timescale²⁵. Zeiss Zen 2.1 software was used to analyze images taken from Zeiss Elyra microscope.

Multifocus image processing. We assembled 3D stacks by aligning the nine simultaneously obtained focal planes on top of one another using bead calibration data as described previously¹⁵. For 3D particle tracking we imported the 16-bit TIFF stack into DiaTrack 3.04 Pro²⁶, which identifies and fits the intensity spots with 3D Gaussian function matched to a predetermined PSF. The following settings were chosen for 3D particle tracking: subtract background, filter data of 1.05, PSF of 1.3 pixels, remove dim of 15, and remove blurred of 0.05. Resulting 3D tracks were exported with code written in Igor Pro 6.36 as one text file containing frame numbers, as well as *x*, *y*, and *z*-coordinates of all detected points. We plotted a map of all detected particle locations in the (*x*, *y*) plane, color coded for height (*z*), and calculated histograms of detected number of particles over the course of 3D sptPALM data acquisitions. Integrated fluorescence intensities from particles detected in the central two focal planes (multifocal planes 4 and 5) were calculated and converted to photon counts using analysis routines written in Igor Pro version 6.36 (ref. 5). Localization errors were calculated using equation (6) in Mortensen *et al.*²⁷

Activation rate measurement. Live U2OS cells expressing either histone H2B-mEos3.2 or histone H2B-HaloTag labeled with ligands **6** and **16** (*n* = 5 cells for each fluorophore) were imaged under concurrent excitation light (561 nm for PA-JF₅₄₉ and mEos3.2; 637 nm for PA-JF₆₄₆) and activation light (405 nm) for 300 s (300 ms per frame). The time constants (τ) were determined by an exponential fit of fluorescence versus time (**Supplementary Fig. 1g** and **Supplementary Fig. 2f**).

On/off ratio and photon-count estimate. The on/off ratio was determined using the method of Wang *et al.*¹³, and a summary of the data is given in **Supplementary Table 1**. Briefly, U2OS cells expressing either TOMM20-mEos3.2 or TOMM20-HaloTag labeled with ligands **6** and **16** were fixed in 4% PFA for 10 min and then washed as described above. The cells were then imaged in PBS with the excitation laser only (561 nm for PA-JF₅₄₉ and mEos3.2; 637 nm for PA-JF₆₄₆; 300 ms per frame; **Supplementary Fig. 1h** and **Supplementary Fig. 2g**). After ~300 frames, the photoactivation laser (405 nm) was turned on, and the intensity was gradually increased until exhaustion of the photoactivation process. Fluorescent spots were counted using custom software (Airlocalize)²⁸. The on rate was computed as the average number of photoactivated spots per frame during the prephotoactivation phase divided by the total number of fluorescent spots detected over the entire movie. To measure the off rate, we first isolated

the spots from the prephotoactivation phase. Within these, spots separated by less than one pixel were assembled in a trajectory corresponding to an individual molecule. The one-pixel threshold value was determined based on the width of the pair-correlation function computed over all spots in the photoactivation phase. We then fitted the distribution of the number of frames n per molecule to an integrated exponential. Equation (1):

$$p(n) = \int_{n-1}^n \frac{1}{\mu} \exp\left(-\frac{u}{\mu}\right) du \quad (1)$$

to obtain μ , the average fluorophore lifetime in frames (the inverse of the off rate). We finally computed the on/off ratio as the product of the on rate by the average fluorophore lifetime. Each value is the average of two to four separate cells. We note our estimate of the on/off ratio mEos3.2 fixed cells is higher than a previous live-cell measurement¹³. This difference in photophysics likely stems from difference in experimental conditions (PBS versus living cell). From these experiments we also computed the total number of detected photons per molecule by summing the spot intensities for each molecule and adjusting the result for the gain conversion factor of the EM-CCD (**Supplementary Fig. 1i**).

Characterization of blinking kinetics of PA-JF₅₄₉-HaloTag ligand during PALM imaging. We selected a section of the PALM imaging movie from the ensconsin–HaloTag–PA-JF₅₄₉ experiment (**Supplementary Fig. 1r**) that featured a low density of emitters. We determined their positions using a 2D Gaussian mask localization algorithm on the maximum intensity projection

of the movie section²⁸. We subsequently ran the same localization software on the individual frames of the movie and generated a time trajectory for each spot identified in the maximum-intensity projection; if a spot was detected on a given frame within one pixel of the spot identified in the maximum projection, it was assumed to represent the same particle, and the corresponding position, intensity, and frame number were included in the time trajectory. We chose a threshold of one pixel to account for drift; based on a cross-correlation analysis, we estimated the drift to contribute less ~0.25 pixel displacement in each dimension over the duration of the movie. We note that our conservative choice of the threshold might result in a small fraction of false-positive blinking events, and therefore our measurements likely slightly overestimate the dyes' propensity to blink. Using the time trajectory of each particle, we isolated and quantified individual blinking events. The resulting statistics demonstrate that PA-JF₅₄₉ fluorophores exhibit little blinking (on average, 1.4 blinking events; **Supplementary Fig. 1t–v**).

21. English, B.P. & Singer, R.H. in *Proc. SPIE, Biosensing and Nanomedicine VIII* (eds. Mohseni, H. et al.) 955008 (SPIE, 2015).
22. Halstead, J.M. et al. *Science* **347**, 1367–1371 (2015).
23. Preibisch, S., Saalfeld, S., Schindelin, J. & Tomancak, P. *Nat. Methods* **7**, 418–419 (2010).
24. Dedecker, P., Duwé, S., Neely, R.K. & Zhang, J. J. *Biomed. Opt.* **17**, 126008 (2012).
25. Katz, Z.B. et al. *eLife* **5**, e10415 (2016).
26. Vallotton, P. & Olivier, S. *Microsc. Microanal.* **19**, 451–460 (2013).
27. Mortensen, K.I., Churchman, L.S., Spudich, J.A. & Flyvbjerg, H. *Nat. Methods* **7**, 377–381 (2010).
28. Lionnet, T. et al. *Nat. Methods* **8**, 165–170 (2011).